Journal of Power Sources 267 (2014) 739–743

Contents lists available at ScienceDirect

Journal of Power Sources

journal homepage: www.elsevier.com/locate/jpowsour

Short communication

Electrochemically induced and orientation dependent crack propagation in single crystal silicon

Chan Soon Kang [a], Seoung-Bum Son [a], Ji Woo Kim [b], Seul Cham Kim [a], Yong Seok Choi [a], Jae Young Heo [a], Soon-Sung Suh [c], Young-Ugk Kim [c], Yeon Yi Chu [d], Jong Soo Cho [d], Se-Hee Lee [b], Kyu Hwan Oh [a, *]

[a] Department of Material Science and Engineering, Seoul National University, Seoul, South Korea
[b] Department of Mechanical Engineering, University of Colorado at Boulder, Boulder, CO 80309, USA
[c] SAMSUNG SDI CO. LTD, Giheung-gu, Yongin-si, Gyeonggi-do 446-577, South Korea
[d] MK Electron, 316-2 Geumeo-ri, Pogok-myeon, Yongin-si, Gyeong gi-do 449-810, South Korea

HIGHLIGHTS

- Stress and strain states are clearly defined for Si wafers during lithiation.
- Li_xSi layer and crystalline Si wafer behave as a thin film composite materials.
- Elastic modulus of c-Si under Li_xSi layer determine the crack propagation behavior.
- <111> Si wafer shows distinguished behavior from <100> and <110> Si wafers.

ARTICLE INFO

Article history:
Received 1 April 2014
Received in revised form
1 June 2014
Accepted 2 June 2014
Available online 11 June 2014

Keywords:
Crack propagate
Silicon wafer
Lithiation/delithiation
Strain energy release

ABSTRACT

This study reports a direct observation on the crack behavior of lithiated Si wafer. Three different Si wafers with <100>, <110> and <111> axes are investigated, to compare the crack behaviors of different orientation Si wafers. Electrochemically induced cracks in each orientated wafer have dissimilar crack behaviors, because the initiations and propagations of cracks are strongly affected by their orientation and strain energy release rate. It is also found that triangular humps and cracks are formed in the (111) wafer, which are discovered for the first time by in this study. Considering that volume expansion, cracks, and pulverizations of Si are the main issues for the commercial use of Si for Li ion battery, this study provides important insight that is relevant to the design of advanced Si anode materials.

1. Introduction

Silicon is a promising material for anodes in Li ion batteries (LIBs), due to its theoretical capacity of ~3500 mAh g^{-1}. To date, this is the highest known among materials [1–4]. Nevertheless, Silicon is not currently used commercially because problems with volume expansion, cracks, and pulverization upon repeated Li insertion-removal cause significant capacity fades as cycles continue [5].

In many cases, cracks can drive a failure of materials, and these phenomena always create new surfaces [6–8]. During crack formation and propagation, increased surface area can enhance the chance of SEI layer formation. Several studies revealed that the SEI layer formation on Si surface impeded Li ion transportation and caused capacity degradation of Si anode [9–11]. Cracks also cause defects among active materials which results in poor electric contact. To improve the cycle ability, these problem should be resolved in Li ion batteries with Si anode.

Several recent investigations using Si wafers for Li ion batteries led to some important experimental findings. Goldman et al. [12] showed clear anisotropic volume expansion along the <110> direction of bulk Si wafer. Lee et al. [13] also used etched Si wafer with nano-pillars. They reported that the anisotropic volume expansion occurs preferentially at {110} surfaces. Another experimental study by Chon et al. [14] provided quantitative information on stresses associated with electrochemically induced phase transformations in crystalline (100) Si and the resulting mechanical damage. They

* Corresponding author. Tel.: +82 2 880 8306.
E-mail address: kyuhwan@snu.ac.kr (K.H. Oh).

http://dx.doi.org/10.1016/j.jpowsour.2014.06.003
0378-7753/

reported the stress value at the crack formation point during delithiation, showing microscopic images where an atomically sharp interface had been introduced between a-Li_xSi layer and crystalline silicon substrate.

Here, we report a direct observation on the crack behavior of Si wafers with <100>, <110> and <111> axes. We introduced focused ion beam (FIB) cross-sectional analyses to observe cracks initiation and propagation in Si wafers with different orientations. The detailed three-dimensional observation of preferred crack orientation provides important insight for the design of advanced Si anode materials.

2. Experimental procedure

Standard types of 2032 half-coin cells were prepared for this experiment, with Li metal foil as a counter electrode. Si wafers were cut to the size of 0.5 cm × 0.5 cm 1 M $LiPF_6$ solution with ethylene carbonate and dimethyl carbonate (EC:DEC) was used as an electrolyte, and a constant current density of 100 μA cm^{-2} was applied for 6 h, for both lithiation and delithiation, respectively. A detailed schematic of the coin cell is shown in Fig. 1.

Disassembly of the coin cells was done in a glove box, filled with Ar gas. An FIB (NOVA200 dual beam system, FEI) equipped with an air-lock chamber was used for the observation of Si wafers, and TEM sample preparation. Definition of the orientation of the Si wafer was possible using the primary flat of each Si wafer. The primary flats of wafers were horizontal to the FESEM images. The air-lock system enables the observation of lithiated Si wafers without exposure to air. This air-lock system maintains an inert environment, while samples are loaded from the glove box into the FIB chamber. Before the ion milling, Pt is deposited on the sample surface in FIB chamber. The role of Pt is to protect of surface morphology and also to obtain clean cross-section image by preventing re-deposition and curtain effect of FIB milling. Details of the sample load and preparations can be found in previous research [10,15,16]. HRTEM (JSM-3000F, JEOL and Tecnai F20, FEI) with 300 and 200 keV was used for detailed observation of the cracks. Lithium insertion was confirmed by voltage profiles of each wafers given in supplementary information and TEM EELS analysis in our additional experiment with higher current [17].

Crack propagation and deformation were analyzed by the following relations. It has been reported that crack formation and propagation by strain energy release rate can be predicted by parameters with the non-dimensionalized stress intensity factor $F(\alpha, \beta)$, and the non-dimensionalized integral of the crack opening displacement $G(\alpha, \beta)$, the so-called strain release rate [18]. Dundurs parameters (α and β) were used for obtaining the values of F and G,

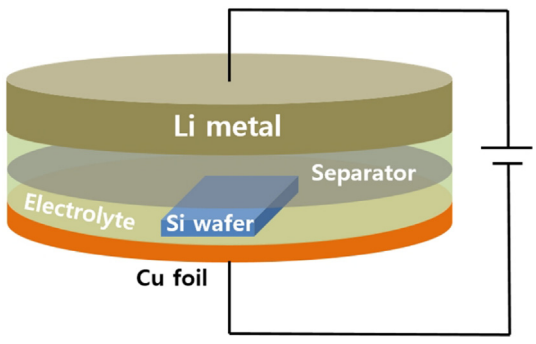

Fig. 1. Schematic of coin cell used in this experiment.

$$F\left(\alpha,\beta,\frac{a}{h}\right)=\frac{K_I}{\sigma(\pi h)^{1/2}},\quad G\left(\alpha,\beta,\frac{a}{h}\right)=\frac{\int_0^a \delta(y)dy}{\pi\frac{\sigma}{E}ah} \tag{1}$$

$$\alpha=\frac{\overline{E_1}-\overline{E_2}}{\overline{E_1}+\overline{E_2}},\quad \beta=\frac{\mu_1(1-2\upsilon_2)-\mu_2(1-2\upsilon_1)}{2\mu_1(1-\upsilon_2)+2\mu_2(1-\upsilon_1)} \tag{2}$$

where, $\overline{E}$ is the material plane strain tensile modulus defined as $E/(1-\nu^2)$, μ is the material shear modulus, K_I is the stress intensity factor, σ is the applied stress, a is the crack length, and h is the film thickness. F and G factors decide whether a crack is taking place or not, and Dundurs parameters can be invoked to explain the crack propagation direction once crack forms because these factors have elastic moduli that are dependent on the material orientation [18,19]. Chow et al. reported that the crack propagations of soft layers on rigid crystalline Si substrate are affected by compliances of each direction of substrate [20]. By using a similar approach, crack propagation could be analyzed by observation in FESEM.

3. Result and discussion

Stress generation during Li insertion and extraction is important in understanding the mechanical failure of Si anode in LIBs. A Li_xSi layer on Si wafer can be treated as a soft layer on rigid substrate (the yield strength of crystalline Si is about 7 GPa and has no plastic deformation; that of lithiated Si is less than 1 GPa, and can be plastically deformed) [14]. It has been known that compressive stress is imparted upon the Li_xSi phase at the reaction front, during Li insertion, while tensile stress is applied to the Li_xSi phase during Li extraction (Fig. 2(b)) [21]. Li_xSi at the surface expands outward upon Li insertion, while the unlithiated Si inside particle constrains Li_xSi at the surface from swelling freely. This results in the unlithiated Si remaining in tensile stress, while lithiated Li_xSi at the reaction front remains in compressive stress. On the other hand, when Li is extracted, the volume of Li_xSi shrinks, and the stress status is reversed as shown in Fig. 2(c).

Fig. 3(a) shows the lithiated (100) Si wafer with parallel lithiated Si layer at the reaction front. This result is consistent with previous results reported by Zhao et al. [21] and Chon et al. [14]. After delithiation, two different kinds of cracks were found from the delithiated (100) Si wafer surface: <110> orientated cracks and <100> oriented cracks as shown in Fig. 3(b and c), respectively.

These directionalities of crack propagations in Fig. 3(b and c) are related to the intrinsic orientation of the Si wafer, and to the strain energy release rate G, as well. For the cracks oriented along the <110> direction in Fig. 3(b), cracks propagate the inside of the wafer, forming an angle of 54.7° to the surface. This angle implies that these cracks propagate along the slip plane {111} in <110> direction inside the Si wafer. The cross-sectional image in Fig. 3(b) also shows that <110> oriented cracks are initiated from the crystalline Si region. As discussed above, tensile stress is applied to the crystalline Si region during lithiation, and then tensile stress in the crystalline Si area initiates and propagates the cracks along the <110> direction on {111} planes [20].

The <100> oriented cracks shown in Fig. 3(c) can be explained by the strain energy release rate G of the crack reaching the critical value of strain energy release rate G_c. In particular with the (100) Si wafer, Li_xSi layer swells upwards much smaller than <110> direction (which is sideward). So lithiated (100) Si wafer can be stated the plane strain ($\varepsilon_x \neq 0$, $\varepsilon_y \neq 0$, $\varepsilon_z \neq 0$). Elastic modulus in plane strain, as so-called the plane strain tensile modulus, was calculated and Chow et al. has reported the values of E_s (Plane strain tensile modulus of Si substrate) for each direction [20]. The E_s values of Si in <100>, <110> and <111> crystal directions are 141.2 GPa,

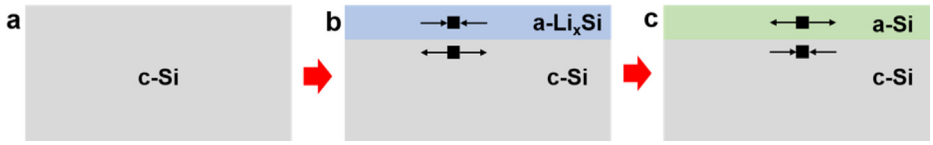

Fig. 2. Schematics of stress field for each status of Si wafer. (a) As-made single crystal Si wafer. (b) Lithiated Si wafer; compressive stress is applied at the lithiated layer, and tensile stress is applied at the crystalline Si substrate. (c) Lithiated/delithiated Si wafer; stress field is applied oppositely to the lithiated Si wafer.

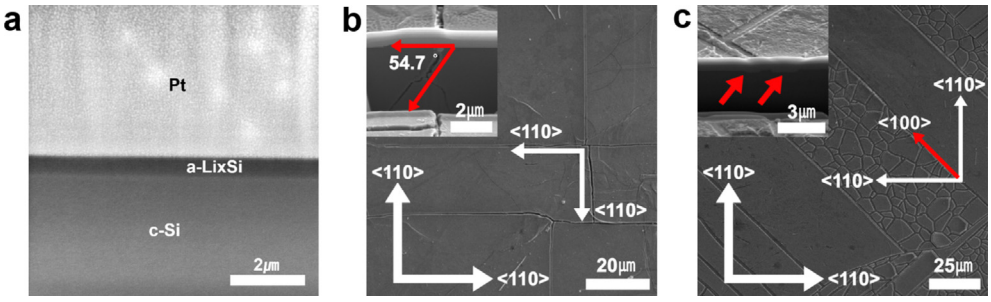

Fig. 3. SEM images of cracks on (100) Si wafer surface after delithiation. (a) Parallel Li insertion to (100) wafer during lithiation. (b) <110> oriented cracks of (100) wafer. (c) <100> and random oriented cracks of (100) wafer.

169.8 GPa, and 181.3 GPa, respectively [20,22]. Upon delithiation, the Li$_x$Si layer at the surface becomes under tensile stress in the <100> wafer. As shown in Fig. 3(c), these <100> oriented cracks (forming an angle of 45° with the <110> direction) on the surface can be initiated, because the <100> direction corresponds to the lowest E_s (the most compliant direction in Si wafer). In other words, cracks can be initiated and propagated easier along <100> direction than others.

In Fig. 4(a), a cross-section of the lithiated (110) Si wafer also shows a-Li$_x$Si layer parallel to the Si wafer substrate. Compared with the lithiated (100) Si wafer in plane strain state, the lithiated (110) wafer is simply in normal strain state. Because the <110> direction is the dominant volume expansion direction upon lithiation, the strain occurs along the 3-axes during lithium insertion into (110) Si wafer. Therefore, the calculated values of elastic moduli are different with plane strain tensile modulus ($\varepsilon_x \neq 0$, $\varepsilon_y \neq 0$, $\varepsilon_z \neq 0$). In this case, both E_{100} and E_{110} are 169 GPa and E_{111} is 181.3 GPa (higher than those (<100> and <110>)) [20,22]. Since (110) Si wafer has anisotropic mechanical properties, a directional crack can be generated based on the strain energy release rate. After lithium extraction, two different types of cracks are observed on the (110) Si wafer surface. Fig. 4(b) shows that the orientations of cracks on the (110) Si wafer surface are mainly in the <100> and <110> directions (forming an angle of 35.2° with the <112> and <111> directions, respectively). These crack propagations can also be explained by the difference in elastic modulus, being defined by compliance in the biaxial stress mode.

It is also found that cracks on the (110) Si wafer (about 400 nm of depth) propagate deeper than those on the (100) Si wafer (about 200 nm of depth). In the (110) wafer, the normal direction from the surface is <110>, which is the fastest Li diffusion direction into Si. This fast diffusion kinetics along the <110> direction is shown as thicker Li$_x$Si layer in (110) wafer than in (100) wafer [23]. Unlike (100) wafer, slip system induced cracks are not observed in the (110) wafer. As discussed, the <110> direction is normal to the surface in the <110> wafer, and the free volume expansion upward is favorable. Consequently, applied stress to the crystalline Si region should be less than for the case of the (100) wafer. Therefore, the applied tensile stress on crystalline (110) Si cannot reach the fracture stress of Si, but can cause the elastic deformation to crystalline Si. As a result, cracks caused by strain energy release are observed, but cracks along the slip system are not observed.

Cracks at the interface between Li$_x$Si and crystalline Si phase in the delithiated (110) Si wafer are observed as shown in Fig. 4(c). This shows crack propagation along the interface between these two phases. According to studies involving detailed observation of lithiated Si, the <110> direction of Si is the preferred direction for Li diffusion into Si, so lithiated Si can freely expand upwards in the (110) wafer [12,13]. After delithiation, the volume of Li$_x$Si is reduced, and the remaining stress is relaxed, as well. Higher tensile

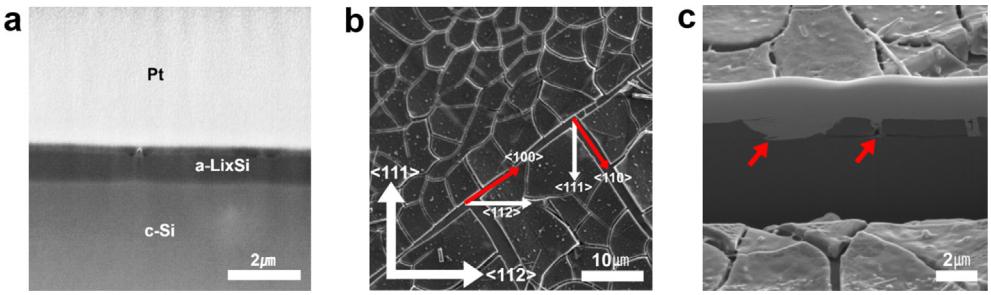

Fig. 4. SEM images of cracks on (110) Si wafer surface, after delithiation. (a) Parallel Li insertion to (110) wafer, during lithiation. (b) <100>, <110>, and random oriented cracks of (110) wafer. (c) Interface cracks between c-Si and a-Si.

stress can be applied between these two phases, and then the interfacial cracks can be initiated. Random direction cracks are likely caused by distributed stress, after cracks are caused by strain energy release.

In Fig. 5(a and b), it is observed that irregular triangular humps are formed on the surface of the (111) wafer, after lithiation. It is analyzed that these triangular humps are only observed in (111) wafer, because of the directionality of <110> in the <111> wafer. In the (111) wafer, there are two possible <110> directions for Li diffusion, which are {111} <110> and {100} <110>, as shown in Fig. 5(c). These <110> orientations form a triangular pyramid shape in the unit cell, and give rise to triangular shapes of Li_xSi phase in the (111) wafer, shown in the cross-sectional image in Fig. 5(b).

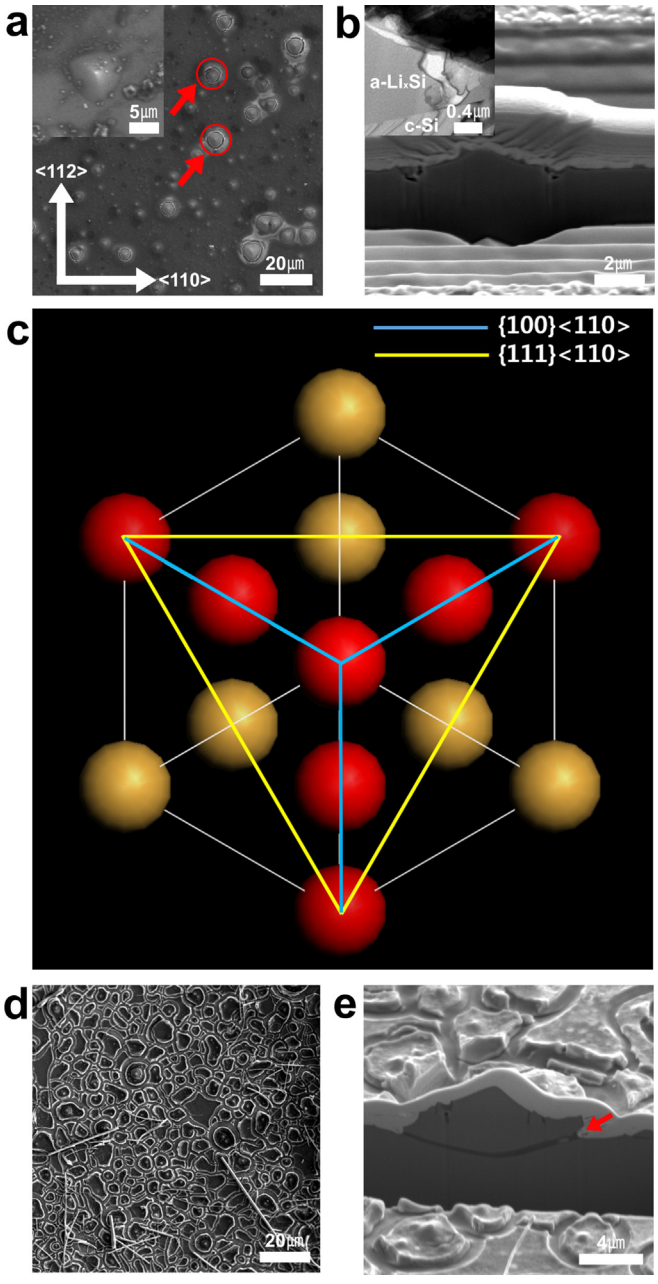

Fig. 5. SEM images of cracks on (111) Si wafer surface, after lithiation and delithiation. (a) (111) Si wafer surface, after lithiation. (b) Cross-sectional image of lithiated hump, and TEM image of hump. (c) Schematic of crystal structure of (111) Si wafer, along the [111] direction. (d) Random oriented cracks of (111) wafer. (e) Crack between c-Si and a-Si, after delithiation.

Once the triangular Li_xSi phase is formed, the free expansion upward is more favorable than breaking new Si bonds and diffusing inside. Therefore, lithiation-induced raised triangular humps can be formed, due to the preferred Li diffusion direction in the (111) Si wafer.

After delithiation, it is observed that cracks are initiated at the edges of humps. Random direction cracks are also formed, as shown in Fig. 5(d). No directional cracks are observed in the (111) Si wafer after delithiation, since the {111} plane is the isotropic structure. Therefore, the strain energy release in all directions at the {111} plane is the same, and this affects the random crack initiation in the (111) Si wafer [17–19]. From the cross-sectional image of the delithiated (111) Si wafer in Fig. 5(e), cracks are observed along the interface between Li_xSi and crystalline Si. However humps still remain after delithiation, which reveals that the humps are the result of plastic deformation, induced by Li insertion into (111) Si wafer.

4. Conclusion

We suggest that the plane strain modulus can be used for uniform lithiation at the {100} plane, and the biaxial modulus is appropriate for the {110} plane of Si, in the case of forming a thin Li_xSi layer at the surface of the wafer. In (100) Si wafer, <110> and <100> oriented cracks are observed, after lithiation/delithiation. We have found that <110> cracks are initiated, and propagated along the slip system of Si and <100> cracks are formed because <100> is the most compliant orientation. In (110) wafer, <100> and <110> oriented cracks are observed, after delithiation. It is known that <100> and <110> have lower elastic modulus than <111>. This difference causes strong directionality of crack propagation in (110) wafer. It can be analyzed that cracks at the delithiated (110) Si wafer are dependent on just the anisotropic properties according to its crystalline orientation (111) wafer shows different morphology changes during lithiation. Li_xSi phase formation occurred, such as humps, and their shape is in response to the direction of volume expansion of lithiated Si. These humps are caused due to the crystallographic characteristics of (111) wafer.

Acknowledgments

This research was supported by a grant from the Fundamental R&D Program for Technology of World Premier Materials, funded by the Ministry of Knowledge Economy, Republic of Korea (10037919). Funding for this study at the University of Colorado was provided by the National Science Foundation (NSF, CHE-1231048). Joost J. Vlassak, who is the current Gordon McKay Professor of Materials Engineering at Harvard University, contributed a discussion to this paper.

Appendix A. Supplementary data

Supplementary data related to this article can be found at http://dx.doi.org/10.1016/j.jpowsour.2014.06.003.

References

[1] M. Armand, J.M. Tarascon, Nature 451 (2008) 652.
[2] R.F.Service, Science 332 (2011) 1494.
[3] J.M. Tarascon, Philos. Trans. R. Soc. A 368 (2010) 3236.
[4] A.S. Arico, P. Bruce, B. Scrosati, J.M. Tarascon, W.V. Schalkwijk, Nat. Mater. 4 (2005) 367.
[5] L.Y. Beaulieu, K.W. Eberman, R.L. Turner, L.J. Krause, J.R. Dahn, Electrochem. Solid-State Lett. 4 (2001) A137.
[6] A. Hellemans, Science 281 (1998) 943.
[7] C. Guerra, J. Scheibert, D. Bonamy, D. Dalmas, PNAS 109 (2012) 390.
[8] A. Livine, E. Bouchbinder, I. Svetlizky, J. Fineberg, Science 327 (2010) 1359.

[9] J. Graetz, C.C. Ahn, R. Yazami, B. Fultz, Electrochem. Solid-State Lett. 6 (2003) A196.
[10] S.B. Son, J.E. Trevey, H. Roh, S.H. Kim, K.B. Kim, J.S. Cho, J.T. Moon, C.M. DeLuca, K.K. Maute, M.L. Dunn, H.N. Han, K.H. Oh, S.H. Lee, Adv. Energy Mater. 1 (2011) 1199.
[11] H. Wu, G. Chan, J.W. Choi, I. Ryu, Y. Yao, M.T. McDowell, S.W. Lee, A. Jackson, Y. Yang, L. Hu, Y. Cui, Nat. Nanotechnol. 7 (2012) 310.
[12] J.L. Goldman, B.R. Long, A.A. Gewirth, R.G. Nuzzo, Adv. Funct. Mater. 21 (2011) 2415.
[13] S.W. Lee, M.T. McDowell, L.A. Berla, D. Nix, Y. Cui, PNAS 109 (2012) 4082.
[14] M.J. Chon, V.A. Sethuraman, A. McCormick, V. Srinivasan, P.R. Guduru, Phys. Rev. Lett. 107 (2011) 045503.
[15] S.B. Son, S.C. Kim, C.S. Kang, T.A. Yersak, Y.C. Kim, C.G. Lee, S.H. Moon, J.S. Cho, J.T. Moon, K.H. Oh, S.H. Lee, Adv. Energy Mater. 2 (2012) 1227.
[16] J.W. Kim, J.P. Ahn, S.A. Jin, S.H. Lee, H.S. Chung, J.H. Shim, Y.H. Cho, K.H. Oh, J. Power Sources 178 (2008) 374.
[17] Y.S. Choi, M. Pharr, C.S. Kang, S.B. Son, S.C. Kim, K.B. Kim, H. Roh, S.H. Lee, K.H. Oh, J.J. Vlassak, J. Power Sources 265 (2014) 160–165.
[18] J.L. Beuth, Int. J. Solids Struct. 29 (1991) 1657–1675.
[19] T. Ye, Z. Suo, A.G. Evans, Int. J. Solids Struct. 29 (1992) 2639–2648.
[20] L.A. Chow, Y.H. Xu, B. Dunn, K.N. Tu, C. Chiang, Appl. Phys. Lett. 73 (1998) 2945.
[21] K. Zhao, M. Pharr, Q. Wan, W.L. Wang, E. Kaxiras, J. Vlassak, Z. Suo, J. Electrochem. 159 (2012) A239.
[22] J.J. Wortman, R.A. Evans, J. Appl. Phys. 36 (1965) 154.
[23] M. Pharr, K. Zhao, X. Wang, Z. Suo, J.J. Vlassak, Nano Lett. 12 (2012) 5043.